Networks and Heterogeneous Media

http://www.aimspress.com/journal/nhm

NHM, 18(4): 1575–1599
DOI: 10.3934/nhm.2023069
Received: 18 May 2023
Revised: 18 July 2023
Accepted: 21 July 2023
Published: 22 August 2023

Research article

A new distributional approach: estimation, Monte Carlo simulation and applications to the biomedical data sets

Mustafa Kamal[1], Meshayil M. Alsolmi[2], Nayabuddin[3], Aned Al Mutairi[4,*], Eslam Hussam[5], Manahil SidAhmed Mustafa[6] and Said G. Nassr[7]

[1] Department of Basic Sciences, College of Science and Theoretical Studies, Saudi Electronic University, Dammam, 32256, Saudi Arabia

[2] Department of Mathematics, College of Science and Arts at Khulis, University of Jeddah, Jeddah, Saudi Arabia

[3] Department of Epidemiology, College of Public Health and Tropical Medicine, Jazan University, Saudi Arabia

[4] Department of Mathematical Sciences, College of Science, Princess Nourah bint Abdulrahman University, P. O. Box 84428, Riyadh 11671, Saudi Arabia

[5] Department of Mathematics, Faculty of Science, Helwan University, Egypt

[6] Department of Statistics, Faculty of Science, University of Tabuk, Tabuk Saudi Arabia

[7] Department of Statistics and Insurance, Faculty of Commerce, Arish University, Al-Arish 45511, Egypt

* **Correspondence:** Email: aoalmutairi@pnu.edu.sa.

Abstract: This paper introduces the generalized exponential-U family of distributions as a novel methodological approach to enhance the distributional flexibility of existing classical and modified distributions. The new family is derived by combining the T-X family method with the exponential model. The paper presents the generalized exponential-Weibull model, an updated version of the Weibull model. Estimators and heavy-tailed characteristics of the proposed method are derived. The new model is applied to three healthcare data sets, including COVID-19 patient survival times and mortality rate data set from Mexico and Holland. The proposed model outperforms other models in terms of analyzing healthcare data sets by evaluating the best model selection measures. The findings suggest that the proposed model holds promise for broader utilization in the area of predicting and modeling healthcare phenomena.

Keywords: Weibull distribution; heavy-tailed distributions; T-X family; healthcare sector; data modeling; China; Mexico; Holland

1. Introduction

The COVID-19 pandemic has been one of the most destructive pandemics of the last few centuries. It has strongly affected every sector globally, including the education sector [1], the healthcare sector [2], the financial sector [3], religious festivals [4], the travel and tourism industry [5], international relations [6], sports affairs [7], show business industries [8], the food supply chain [9] and agricultural markets [10].

Among the above sectors, the healthcare sector has been the most affected by the COVID-19 pandemic as millions of persons have died around the globe. Based on updates up to January 16, 2022, 18:12 GMT, 327.6 million COVID-19 cases and 5.56 million deaths have been registered around the globe, while 266.99 million infected people have recovered. For a comparison of COVID-19 events in Asian countries, refer to [11]. For a comparison of the COVID-19 events in 189 different countries, refer to [12]. Furthermore, the authors of [13] looked at the distribution of COVID-19 in different selected countries during different phases of the pandemic. They provide a "horse race of sorts" that compares various distributions, as well as various mixtures of distributions. They also present an extensive review of the literature, considering COVID-19 mortality and morbidity.

Around the globe, the top 10 countries with the largest number of confirmed COVID-19 cases (registered cases) as of January 16, 2022 are (i) the USA, with 66,712,140 registered cases; (ii) India, with 37,122,164 registered cases; (iii) Brazil, with 22,975,723 registered cases; (iv) the UK, with 15,217,280 registered cases; (v) France, with 13,894,255 registered cases; (vi) Russia, with 10,803,534 registered cases; (vii) Turkey, with 10,457,164 registered cases; (viii) Italy with 8,698,962 registered cases; (ix) Spain, with 8,093,036 registered cases; and (x) Germany, with 7,977,550 registered cases. In contrast, the top 10 countries with the most total COVID-19 deaths (registered deaths) are (i) the USA, with 873,215 registered deaths; (ii) Brazil, with 621,007 registered deaths; (iii) India, with 486,094 registered deaths; (iv) Russia, with 321,320 registered deaths; (v) Mexico, with 301,334 registered deaths; (vi) Peru, with 203,376 registered deaths; (vii) the UK, with 151,987 registered deaths; (viii) Indonesia, with 144,170 registered deaths; (ix) Italy, with 141,104 registered deaths; and (x) Iran, with 132,075 registered deaths. For more, see https://www.worldometers.info/coronavirus/.

Owing to the serious effects of the COVID-19 pandemic on the health sector, it is crucial to learn more about this deadly pandemic. In this regard, numerous statistical methods have been introduced and implemented to predict and model COVID-19 behavior (events or data); see [14–21].

As we know, extreme distribution theory, including heavy-tailed (HT) and long-range dependence, is a current area of active research due to its importance in a vast range of applications as well as its violation of classical assumptions. The readers are referred to [22, 23] and their citations for precise definitions of these effects as well as the current state of theory in this area. Particularly, the HT distributions offer satisfactory performance when applied to health-related sectors [24]. However, only a limited number of probability models possess HT characteristics. As of my last update in September 2021, researchers were indeed exploring and developing new probability distributions with HT characteristics. HT distributions are statistical distributions with more significant probabilities of extreme events or outliers than normal distributions. They are characterized by slowly decaying tails and a higher likelihood of extreme values.

These distributions have gained attention in various fields, including finance, economics, telecommunications and other domains where extreme events play a crucial role. Traditional probability distributions, such as the Gaussian (normal) distribution, are not suitable for modeling HT data, as they underestimate the likelihood of extreme events.

Some of the well-known HT distributions include the following:

1. Cauchy distribution: It has a very heavy tail and lacks a defined mean and variance.

2. Student's t-distribution: It is frequently employed to estimate the mean of a normally distributed population in cases in which the sample size is limited. Additionally, it displays fat tails.

3. Pareto distribution: Often used to model income and wealth distributions, this distribution has a power-law tail.

4. Generalized Pareto distribution: It is an extension of the Pareto distribution, often used to model extreme values.

5. Levy distribution: It is characterized by infinite variance and heavy tails.

Researchers might have been working on novel HT distributions or refining existing ones to better capture extreme events in real-world data. Additionally, they could explore these distributions' applications in various fields, develop estimation methods and study their theoretical properties.

We recommend checking recent research papers and articles in relevant scientific journals and conferences for the most up-to-date information on specific developments in probability distributions with HT characteristics; see [25, 26].

Due to the usefulness of HT distributions in medical and other practical fields, we make a significant contribution to this research domain by introducing a new approach (or family of distributions) that exhibits HT characteristics. This novel method is referred to as the generalized exponential-U (GE-U) family of distributions. The GE-U method is derived through a combination of the T-X method and the exponential model with the probability density function (PDF) defined as $w(t) = e^{-t}$. The following section presents the derivation of the proposed GE-U distributions.

2. Development of the GE-U family

Assume that $T \in \mathbb{R}$ is a random variable (RV) with the PDF $w(t)$, where $T \in [\phi_1, \phi_2]$ for $-\infty \leq \phi_1 < \phi_2 \leq \infty$. Let X be an RV with the cumulative distribution function (CDF) $U(x;\boldsymbol{\psi})$ that is dependent on a parameter vector $\boldsymbol{\psi}$. Now, consider a function of $U(x;\boldsymbol{\psi})$, denoted by $M[U(x;\boldsymbol{\psi})]$, satisfying the following three conditions:

(*i*) $M[U(x;\boldsymbol{\psi})] \in [\phi_1, \phi_2]$,
(*ii*) $M[U(x;\boldsymbol{\psi})]$ is differentiable as well as a monotonically increasing function,
(*iii*) $M[U(x;\boldsymbol{\psi})] \to \phi_1$ as $x \to -\infty$ and $M[U(x;\boldsymbol{\psi})] \to \phi_2$ as $x \to \infty$.

The CDF of the T-X approach of [27] is defined by

$$K(x;\boldsymbol{\psi}) = \int_{\phi_1}^{M[U(x;\boldsymbol{\psi})]} w(t)\,dt, \qquad x \in \mathbb{R}, \tag{2.1}$$

with the PDF $k(x;\boldsymbol{\psi})$

$$k(x;\boldsymbol{\psi}) = \left\{\frac{d}{dx}M[U(x;\boldsymbol{\psi})]\right\} w\{M[U(x;\boldsymbol{\psi})]\}, \qquad x \in \mathbb{R}.$$

For more about the T-X method, we refer the reader to [28].

Let $T > 0$ follow the exponential distribution with the parameter $\theta > 0$, if its CDF is given by

$$W(t) = 1 - e^{-\theta t} \tag{2.2}$$

Using $\theta = 1$ in Eq (2.2), we can find that

$$W(t) = 1 - e^{-t} \tag{2.3}$$

Corresponding to Eq (2.3), the PDF $w(t)$, can be written as

$$w(t) = e^{-t} \tag{2.4}$$

Here, we implement the T-X method to introduce the GE-U family of distributions. The GE-U family is introduced by replacing $M[U(x;\boldsymbol{\psi})] = -\log\left(\frac{\varphi^2[1-U(x;\boldsymbol{\psi})]}{[\varphi-U(x;\boldsymbol{\psi})]^2}\right)$ and using Eq (2.4) in Eq (2.1). Let X follow the GE-U family; then, its DF is given by

$$K(x;\varphi,\boldsymbol{\psi}) = 1 - \frac{\varphi^2 \bar{U}(x;\boldsymbol{\psi})}{[\varphi - U(x;\boldsymbol{\psi})]^2}, \qquad \varphi > 2, \varphi < 0, x \in \mathbb{R} \tag{2.5}$$

where, $\bar{U}(x;\boldsymbol{\psi}) = 1 - U(x;\boldsymbol{\psi})$ is the survival function (SF) of the baseline model. It is important to note that the DF in Eq (2.5) is only true if $\varphi > 2$ and $\varphi < 0$. The step-by-step derivation of Eq (2.5) is provided in Appendix A.

By searching for and studying the literature on distribution theory, we observed that the GE-U method has not been proposed or used so far. This is one of the reasons to study the GE-U method. Regarding $K(x;\varphi,\boldsymbol{\psi})$ as provided in Eq (2.5), the PDF $k(x;\varphi,\boldsymbol{\psi})$ is given by

$$k(x;\varphi,\boldsymbol{\psi}) = \frac{\varphi^2 u(x;\boldsymbol{\psi})}{[\varphi - U(x;\boldsymbol{\psi})]^3}[\varphi - 2 + U(x;\boldsymbol{\psi})], \qquad x \in \mathbb{R} \tag{2.6}$$

where $\frac{d}{dx}U(x;\boldsymbol{\psi}) = u(x;\boldsymbol{\psi})$.

Regarding $K(x;\varphi,\boldsymbol{\psi})$ as provided in Eq (2.5) and the PDF $k(x;\varphi,\boldsymbol{\psi})$ presented in Eq (2.6), the SF $S(x;\varphi,\boldsymbol{\psi}) = 1 - K(x;\varphi,\boldsymbol{\psi})$ and hazard function (HF) $h(x;\varphi,\boldsymbol{\psi}) = \frac{k(x;\varphi,\boldsymbol{\psi})}{1-K(x;\varphi,\boldsymbol{\psi})}$ are given, respectively, by

$$S(x;\varphi,\boldsymbol{\psi}) = \frac{\varphi^2 \bar{U}(x;\boldsymbol{\psi})}{[\varphi - U(x;\boldsymbol{\psi})]^2}, \qquad x \in \mathbb{R}$$

and

$$h(x;\varphi,\boldsymbol{\psi}) = \frac{u(x;\boldsymbol{\psi})}{\bar{U}(x;\boldsymbol{\psi})[\varphi - U(x;\boldsymbol{\psi})]}[\varphi - 2 + U(x;\boldsymbol{\psi})], \qquad x \in \mathbb{R}$$

The primary advantage of the proposed GE-U method is its adherence to the characteristics of HT distributions. This feature offers the method an excellent fit to data sets exhibiting HT behavior. In practical terms, it means that the GE-U method can effectively model and capture the statistical properties of data sets with heavy tails, making it a valuable tool in various applications wherein such distributions are encountered.

However, the GE-U method has certain disadvantages too. The disadvantages of the GE-U method are that (i) its distribution function is not in an explicit form and (ii) the form of the PDF of the GE-U method is complicated. Therefore, obtaining various distributional properties of the mentioned probability distribution demands increased computational efforts and extensive mathematical work.

In the following section, we explain an application of the GE-U method to present a broadened and extended form of the Weibull distribution. This newly introduced variant is referred to as the generalized exponential-Weibull (GE-Weibull) distribution. The subsequent section will present detailed expressions for the CDF and PDF of the GE-Weibull model.

3. The GE-Weibull model: a special model

Let us assume that the DF $U(x;\boldsymbol{\psi})$ and PDF $u(x;\boldsymbol{\psi})$ of the Weibull distribution are provided as follows:

$$U(x;\boldsymbol{\psi}) = 1 - e^{-\lambda x^{\delta}}, \qquad x \geq 0, \delta, \lambda \in \mathbb{R}^{+} \tag{3.1}$$

and

$$u(x;\boldsymbol{\psi}) = \delta\lambda x^{\delta-1} e^{-\lambda x^{\delta}}$$

respectively, where $\boldsymbol{\psi} = (\delta, \lambda)$. The DF of the GE-Weibull model is derived by integrating Eq (3.1) into Eq (2.5). We can say that $K(x;\varphi,\boldsymbol{\psi})$ is given by

$$K(x;\varphi,\boldsymbol{\psi}) = 1 - \frac{\varphi^2 e^{-\lambda x^{\delta}}}{\left[\varphi - 1 + e^{-\lambda x^{\delta}}\right]^2}, \qquad x \geq 0 \tag{3.2}$$

According to Eq (3.2), the PDF is expressed as follows:

$$k(x;\varphi,\boldsymbol{\psi}) = \frac{\varphi^2 \delta\lambda x^{\delta-1} e^{-\lambda x^{\delta}}}{\left[\varphi - 1 + e^{-\lambda x^{\delta}}\right]^3}\left[\varphi - 1 - e^{-\lambda x^{\delta}}\right] \tag{3.3}$$

Figure 1 displays various graphs representing $k(x;\varphi,\boldsymbol{\psi})$ of the GE-Weibull model, as defined in Eq (3.3), for different scenarios:

(*i*) $\delta = 1.3, \lambda = 1.0, \varphi = 200$ (gold curve line); (*ii*) $\delta = 1.3, \lambda = 0.8, \varphi = 500$ (green curve line); (*iii*) $\delta = 1.3, \lambda = 0.6, \varphi = 9000$ (blue curve line); (*iv*) $\delta = 1.3, \lambda = 0.4, \varphi = 12000$ (red curve line); and (*iii*) $\delta = 1.3, \lambda = 0.3, \varphi = 15000$ (black curve line).

The plots of $k(x;\varphi,\boldsymbol{\psi})$ in Figure 1 illustrate that as the value of λ decreases and the value of φ increases, the GE-Weibull distribution behaves like the HT distribution.

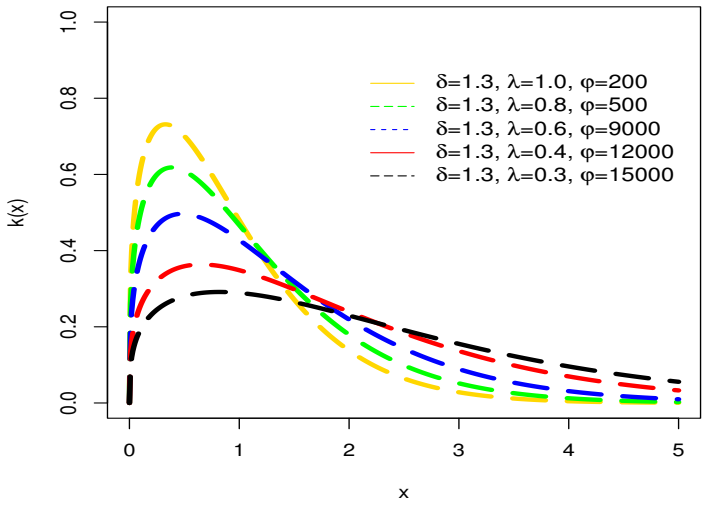

Figure 1. The plots of $f(x;\varphi,\boldsymbol{\psi})$ for different values of δ, λ and φ.

Furthermore, the SF $S(x;\varphi,\boldsymbol{\psi})$ and HF $h(x;\varphi,\boldsymbol{\psi})$ of the GE-Weibull model are given by

$$S(x;\varphi,\boldsymbol{\psi}) = \frac{\varphi^2 e^{-\lambda x^{\delta}}}{\left[\varphi - 1 + e^{-\lambda x^{\delta}}\right]^2}, \qquad x > 0$$

and

$$h(x;\varphi,\boldsymbol{\psi}) = \frac{\varphi^2 \delta \lambda x^{\delta-1}}{\left[\varphi - 1 + e^{-\lambda x^{\delta}}\right]^3}\left[\varphi - 1 - e^{-\lambda x^{\delta}}\right], \qquad x > 0$$

respectively.

Different plots of $h(x;\varphi,\boldsymbol{\psi})$ for the GE-Weibull model are shown in Figure 2. The HF plots for the GE-Weibull model are shown for (*i*) $\delta = 0.3, \lambda = 1.5, \varphi = 2.5$ (red curve line); (*ii*) $\delta = 2.2, \lambda = 0.1, \varphi = 2.1$ (green curve line); and (*iii*) $\delta = 0.2, \lambda = 0.9, \varphi = 3.5$ (gold curve line).

The plots of $h(x;\varphi,\boldsymbol{\psi})$ in Figure 2 reveal that the GE-Weibull distribution can capture three possible patterns, i.e., (*i*) decreasing (red curve line), (*ii*) bathtub (gold curve line) and (*iii*) increasing (green curve line). The plots of $h(x;\varphi,\boldsymbol{\psi})$ in Figure 2 show that the GE-Weibull distribution is more flexible than the Weibull distribution as it captures the monotonic hazard shapes such as the decreasing and increasing hazard shapes. Besides the monotonic hazard shapes, the GE-Weibull distribution also captures the bathtub hazard shape, which is a very crucial monotonic hazard shape.

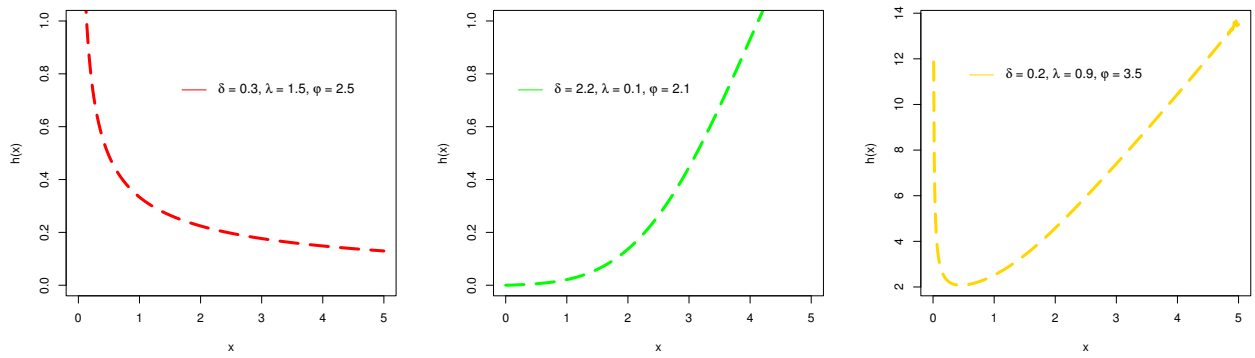

Figure 2. The plots of $h(x;\varphi,\boldsymbol{\psi})$ for the GE-Weibull distribution.

Furthermore, different plots of $K(x;\varphi,\boldsymbol{\psi})$ for the GE-Weibull distribution are shown in Figure 3. These plots are shown for different values of δ, λ and φ.

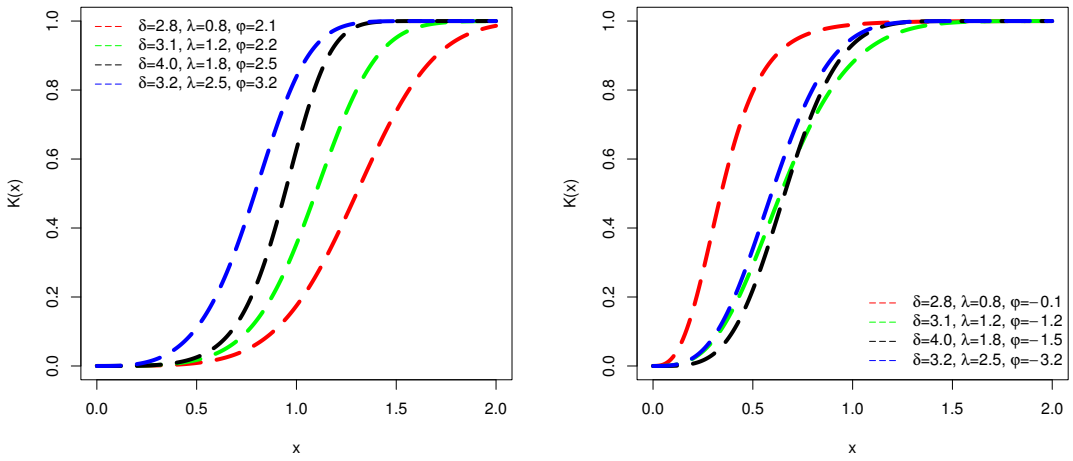

Figure 3. The plots of $K(x;\varphi,\boldsymbol{\psi})$ for the GE-Weibull distribution for different values of δ, λ and φ.

The plots in Figures 1–3 were obtained by using the R-programming software. As an example, the R code for the plots of the DF for the proposed model is provided in Appendix B.

4. The HT characteristics of the GE-U distributions

The section offers a complete mathematical treatment to prove the HT characteristics of the GE-U distributions.

4.1. The regularly varying tail behavior

The importance of regularly varying tail behavior (ReVaTB) cannot be understated when identifying HT distributions [29]. In this context, we calculate the ReVaTB of the GE-U distributions.

As indicated in [30], this is expressed in terms of the SF $\bar{U}(x;\boldsymbol{\psi})$.

Theorem 1: If $S(x;\boldsymbol{\psi}) = 1 - U(x;\boldsymbol{\psi})$ is a regularly varying function (RaVaF), then $S(x;\varphi,\boldsymbol{\psi}) = 1 - M(x;\psi,\boldsymbol{\psi})$ is also a RaVaF.

Proof. Assume that $\lim_{x\to\infty} \frac{S(px;\boldsymbol{\psi})}{S(x;\boldsymbol{\psi})} = n(p)$ is a finite function that is nonzero and that $\forall\ p > 0$. Using Eq (2.5), we have

$$\frac{S\left(px;\varphi,\boldsymbol{\psi}\right)}{S\left(x;\varphi,\boldsymbol{\psi}\right)} = \frac{\varphi^2\left[1 - U\left(px;\boldsymbol{\varphi}\right)\right]}{\left[\varphi - U\left(px;\boldsymbol{\psi}\right)\right]^2} \times \frac{\left[\varphi - U\left(x;\boldsymbol{\psi}\right)\right]^2}{\varphi^2\left[1 - U\left(x;\boldsymbol{\psi}\right)\right]},$$

$$\frac{S\left(px;\varphi,\boldsymbol{\psi}\right)}{S\left(x;\varphi,\boldsymbol{\psi}\right)} = \frac{\left[1 - U\left(px;\boldsymbol{\psi}\right)\right]}{\left[1 - U\left(x;\boldsymbol{\psi}\right)\right]} \times \frac{\left[\varphi - U\left(x;\boldsymbol{\psi}\right)\right]^2}{\left[\varphi - U\left(px;\boldsymbol{\psi}\right)\right]^2} \tag{4.1}$$

Taking $\lim_{x\to\infty}$ on both sides of Eq (4.1), we get

$$\lim_{x\to\infty} \frac{S\left(px;\varphi,\boldsymbol{\psi}\right)}{S\left(x;\varphi,\boldsymbol{\psi}\right)} = \lim_{x\to\infty} \frac{\left[1 - U\left(px;\boldsymbol{\psi}\right)\right]}{\left[1 - U\left(x;\boldsymbol{\psi}\right)\right]} \times \frac{\left[\varphi - U\left(x;\boldsymbol{\psi}\right)\right]^2}{\left[\varphi - U\left(px;\boldsymbol{\psi}\right)\right]^2} \tag{4.2}$$

Because $\lim_{x\to\infty} U\left(x;\boldsymbol{\psi}\right) = 1$, from Eq (4.2), we get

$$\lim_{x\to\infty} \frac{S\left(px;\varphi,\boldsymbol{\psi}\right)}{S\left(x;\varphi,\boldsymbol{\psi}\right)} = \lim_{x\to\infty} \frac{\left[1 - U\left(px;\boldsymbol{\psi}\right)\right]}{\left[1 - U\left(x;\boldsymbol{\psi}\right)\right]} \times \frac{\left[\varphi - U\left(\infty;\boldsymbol{\psi}\right)\right]^2}{\left[\varphi - U\left(p.\infty;\boldsymbol{\psi}\right)\right]^2},$$

$$\lim_{x\to\infty} \frac{S\left(px;\varphi,\boldsymbol{\psi}\right)}{S\left(x;\varphi,\boldsymbol{\psi}\right)} = \lim_{x\to\infty} \frac{\left[1 - U\left(px;\boldsymbol{\psi}\right)\right]}{\left[1 - U\left(x;\boldsymbol{\psi}\right)\right]} \times \frac{\left[\varphi - U\left(\infty;\boldsymbol{\psi}\right)\right]^2}{\left[\varphi - U\left(\infty;\boldsymbol{\psi}\right)\right]^2},$$

$$\lim_{x\to\infty} \frac{S\left(px;\varphi,\boldsymbol{\psi}\right)}{S\left(x;\varphi,\boldsymbol{\psi}\right)} = \lim_{x\to\infty} \frac{\left[1 - U\left(px;\boldsymbol{\psi}\right)\right]}{\left[1 - U\left(x;\boldsymbol{\psi}\right)\right]} \times \frac{\left[\varphi - 1\right]^2}{\left[\varphi - 1\right]^2},$$

$$\lim_{x\to\infty} \frac{S\left(px;\varphi,\boldsymbol{\psi}\right)}{S\left(x;\varphi,\boldsymbol{\psi}\right)} = \lim_{x\to\infty} \frac{S\left(px;\boldsymbol{\psi}\right)}{S\left(x;\boldsymbol{\psi}\right)},$$

$$\lim_{x\to\infty} \frac{S\left(px;\varphi,\boldsymbol{\psi}\right)}{S\left(x;\varphi,\boldsymbol{\psi}\right)} = n\left(p\right) \tag{4.3}$$

We can see that Eq (4.3) is non-zero and finite and that $\forall\ p > 0$. Thus, $S\left(x;\varphi,\boldsymbol{\psi}\right)$ is a RaVaF.

4.2. The regular variational result

Let X follow a power law characteristic; then, we have

$$S\left(x;\boldsymbol{\psi}\right) = 1 - U\left(x;\boldsymbol{\psi}\right) = \mathbb{P}(X > x) \sim x^{-\theta}$$

Now, by incorporating the findings of Karamata's theorem, we can write $S\left(x;\varphi,\boldsymbol{\psi}\right)$ as

$$S\left(x;\varphi,\boldsymbol{\psi}\right) = x^{-\theta}L(x)$$

where $L(x)$ represents a slowly varying function (VaF). Note that

$$S\left(x;\varphi,\boldsymbol{\psi}\right)=\frac{\varphi^{2}\left[1-U\left(x;\boldsymbol{\psi}\right)\right]}{\left[\varphi-U\left(x;\boldsymbol{\psi}\right)\right]^{2}} \tag{4.4}$$

Because $1-U\left(x;\boldsymbol{\psi}\right)\sim x^{-\theta}$, from the expression in Eq (4.4), we get

$$S\left(x;\varphi,\boldsymbol{\psi}\right)=\frac{\varphi^{2}x^{-\theta}}{\left(\varphi-x^{-\theta}\right)^{2}}$$

$$S\left(x;\varphi,\boldsymbol{\psi}\right)=x^{-\varphi}L\left(x\right)$$

where $L(x)=\frac{\varphi^{2}}{\left(\varphi-x^{-\theta}\right)^{2}}$. Accordingly, if we can show that $L(x)$ is a slow VaF, then the RaVaTB derived above is true. Using the results of [31], $\forall\ \theta>0$ and we must show that

$$\lim_{x\to\infty}\frac{L(px)}{L(x)}=1 \tag{4.5}$$

After conducting further computational analysis, we have obtained the following results:

$$\frac{L(px)}{L(x)}=\frac{\varphi^{2}}{\left(\varphi-(px)^{-\theta}\right)^{2}}\times\frac{\left(\varphi-x^{-\theta}\right)^{2}}{\varphi^{2}},$$

$$\frac{L(px)}{L(x)}=\frac{\left(\varphi-x^{-\theta}\right)^{2}}{\left(\varphi-(px)^{-\theta}\right)^{2}} \tag{4.6}$$

Now, taking $\lim_{x\to\infty}$ on both sides of Eq (4.6), we get

$$\lim_{x\to\infty}\frac{L(px)}{L(x)}=\frac{\left(\varphi-x^{-\theta}\right)^{2}}{\left(\varphi-(px)^{-\theta}\right)^{2}} \tag{4.7}$$

Because $x\to\infty$, $\lim_{x\to\infty}\frac{1}{x^{\theta}}=0$ and $\lim_{x\to\infty}\frac{1}{x^{\theta}p^{\theta}}=0$. So from Eq (4.6), we get

$$\lim_{x\to\infty}\frac{L(px)}{L(x)}=\frac{\varphi^{2}}{\varphi^{2}}$$

Finally, we are led to the proof of Eq (4.7), given by

$$\lim_{x\to\infty}\frac{L(px)}{L(x)}=1 \tag{4.8}$$

Since the expression in Eq (4.8) is identical to Eq (4.5), we can say that $L(x)$ is a slow VaF.

5. Estimation and simulation

This section describes the derivation of the maximum likelihood estimators (MLES) $\left(\hat{\varphi}_{MLE},\hat{\boldsymbol{\psi}}_{MLE}\right)$ of the parameters $(\varphi,\boldsymbol{\psi})$. After computing $\hat{\varphi}_{MLE}$ and $\hat{\boldsymbol{\psi}}_{MLE}$, a simulation study (SiSt) was conducted to assess the performances of $\hat{\varphi}_{MLE}$ and $\hat{\boldsymbol{\psi}}_{MLE}$.

5.1. Estimation

Consider a set of random samples (RS) of size of n, say $X_1, X_2, ..., X_n$, taken from $k(x;\varphi,\boldsymbol{\psi})$. Then, regarding $k(x;\varphi,\boldsymbol{\psi})$, the likelihood function (LiF) expressed by $\kappa(\varphi,\boldsymbol{\psi}|x_1, x_2, ..., x_n)$ is given by

$$\kappa(\varphi,\boldsymbol{\psi}|x_1, x_2, ..., x_n) = \prod_{b=1}^{n} k(x_b;\varphi,\boldsymbol{\psi}) \tag{5.1}$$

Incorporating Eq (2.6) in Eq (5.1), we have

$$\kappa(\varphi,\boldsymbol{\psi}|x_1, x_2, ..., x_n) = \prod_{b=1}^{n} \frac{\varphi^2 u(x_b;\boldsymbol{\psi})}{[\varphi - U(x_b;\boldsymbol{\psi})]^3}[\varphi - 2 + U(x_b;\boldsymbol{\psi})]$$

Corresponding to $\kappa(\varphi,\boldsymbol{\psi}|x_1, x_2, ..., x_n)$, the log LiF $\eta(x_1, x_2, ..., x_n|\varphi,\boldsymbol{\psi})$ is given by

$$\eta(x_1, x_2, ..., x_n|\varphi,\boldsymbol{\psi}) = 2\log\varphi + \sum_{b=1}^{n}\log u(x_b;\boldsymbol{\psi}) + \sum_{b=1}^{n}\log[\varphi - 2 + U(x_b;\boldsymbol{\psi})] - 3\sum_{b=1}^{n}\log[\varphi - U(x_b;\boldsymbol{\psi})]$$

In connection with $\eta(x_1, x_2, ..., x_n|\varphi,\boldsymbol{\psi})$, the partial derivatives of the given expression with respect to φ and $\boldsymbol{\psi}$ are as follows:

$$\frac{\partial}{\partial\varphi}\eta(x_1, x_2, ..., x_n|\varphi,\boldsymbol{\psi}) = \frac{2}{\varphi} + \sum_{b=1}^{n}\frac{1}{[\varphi - 2 + U(x_b;\boldsymbol{\psi})]} - \sum_{b=1}^{n}\frac{3}{[\varphi - U(x_b;\boldsymbol{\psi})]}, \tag{5.2}$$

and

$$\frac{\partial}{\partial\boldsymbol{\psi}}\eta(x_1, x_2, ..., x_n|\varphi,\boldsymbol{\psi}) = \sum_{b=1}^{n}\frac{\frac{\partial}{\partial\boldsymbol{\psi}}u(x_b;\boldsymbol{\psi})}{u(x_b;\boldsymbol{\psi})} + \sum_{b=1}^{n}\frac{\frac{\partial}{\partial\boldsymbol{\psi}}U(x_b;\boldsymbol{\psi})}{[\varphi - 2 + U(x_b;\boldsymbol{\psi})]} - 3\sum_{b=1}^{n}\frac{\frac{\partial}{\partial\boldsymbol{\psi}}U(x_b;\boldsymbol{\psi})}{[\varphi - U(x_b;\boldsymbol{\psi})]} \tag{5.3}$$

respectively.

Solving $\frac{\partial}{\partial\varphi}\eta(x_1, x_2, ..., x_n|\varphi,\boldsymbol{\psi}) = 0$ and $\frac{\partial}{\partial\boldsymbol{\psi}}\eta(x_1, x_2, ..., x_n|\varphi,\boldsymbol{\psi}) = 0$, yields $\hat{\varphi}_{MLE}$ and $\hat{\boldsymbol{\psi}}_{MLE}$ respectively.

From the expressions in Eqs (5.2) and (5.3), it is obvious that the MLEs $\left(\hat{\varphi}_{MLE}, \hat{\boldsymbol{\psi}}_{MLE}\right)$ of (φ,ψ) are not in an explicit form. Therefore, they cannot be obtained analytically and we must use an iterative procedure such as the Newton-Raphson method to obtain the MLEs of φ and ψ numerically.

In the next section, we use the `optim()` R-function with a well-known algorithm, i.e., `method = "SANN"` to obtain the numerical values of the MLEs of the GE-Weibull distribution.

5.2. Simulation

Regarding this part of the paper, we describe a numerical study conducted to assess the performances of $\hat{\varphi}_{MLE}$ and $\hat{\boldsymbol{\psi}}_{MLE}$ via a SiSt. To carry out the SiSt, we adopted the inverse DF (quantile function) method to obtain the random numbers (RNs) from the GE-U distributions with the DF $K(x;\varphi,\boldsymbol{\psi})$ and PDF $K(x;\varphi,\boldsymbol{\psi})$.

The SiSt was carried out for two sets of δ,λ and φ, i.e., (a) $\delta = 0.7, \varphi = 2.1, \lambda = 1$ and (b) $\delta = 0.8, \varphi = 2.2, \delta = 1, \lambda = 1.2$. For both sets of combination values of δ,λ and φ presented in (a) and (b), an RS of the sizes n = 35, 70, 105, ..., 700 were obtained by using the formula

$$Q(v) = (1-v)\,U(x;\boldsymbol{\psi})^2 + \left(\varphi^2 - 2\varphi(1-v)\right)U(x;\boldsymbol{\psi}) - \varphi v = 0$$

where $v \in (0,1)$.

For each combination value of δ,λ and φ, the simulation process was repeated N = 700 times. The performances of $\hat{\varphi}_{MLE}$ and $\hat{\boldsymbol{\psi}}_{MLE}$ were evaluated by calculating two statistical measures: (i) the biases and (ii) the mean square error (MSE). The mathematical expressions of these measures are given by

$$Bias\left(\hat{\boldsymbol{\Delta}}\right) = \frac{1}{N}\sum_{b=1}^{N}\left(\hat{\boldsymbol{\Delta}} - \boldsymbol{\Delta}\right)$$

and

$$MSE\left(\hat{\boldsymbol{\Delta}}\right) = \frac{1}{N}\sum_{b=1}^{N}\left(\hat{\boldsymbol{\Delta}} - \boldsymbol{\Delta}\right)^2$$

respectively, where $\boldsymbol{\Delta} = (\varphi,\boldsymbol{\psi})$.

For (a) $\delta = 0.7, \varphi = 2.1, \lambda = 1$ and (b) $\delta = 0.8, \varphi = 2.2, \delta = 1, \lambda = 1.2$, the results of the SiSt for the GE-Weibull model are respectively summarized in Tables 1 and 2. These tables provide information on the estimated values of the parameters

Moreover, Figures 4 and 5 display graphical representations of the SiSt outcomes. Figure 4 illustrates the performance of the MLEs.

These visual representations complement the tabulated results and clarify how the estimators perform under various conditions and sample sizes. The combination of tables and figures contributes to a comprehensive assessment of the GE-Weibull model's fitting and the reliability of the MLEs in terms of capturing the model's parameters.

From Table 1, Table 2, Figure 4 and Figure 5, we can easily observe the following:

- The MLEs $\left(\hat{\delta}_{MLE}, \hat{\lambda}_{MLE}, \hat{\varphi}_{MLE}\right)$ tend to stable as n increases.
- The MSEs of $\hat{\delta}_{MLE}, \hat{\lambda}_{MLE}$ and $\hat{\varphi}_{MLE}$ decrease as n increases.
- The biases of $\hat{\delta}_{MLE}, \hat{\lambda}_{MLE}$ and $\hat{\varphi}_{MLE}$ decay to zero as n increases.

Table 1. The simulation results of the GE-Weibull distribution.

n	Par.	MLE	MSEs	Biases
35	δ	0.7518305	0.02247213	0.05183051
	φ	2.9472000	4.09630218	0.84719998
	λ	1.4653645	2.00189631	0.46536453
70	δ	0.7404539	0.01351612	0.04045387
	φ	2.8713390	3.19850410	0.77133907
	λ	1.1695551	0.74498885	0.16955511
105	δ	0.7374223	0.00887764	0.03742227
	φ	2.7470570	2.31273869	0.64705656
	λ	1.0241156	0.22840275	0.02411562
140	δ	0.7347455	0.00684264	0.03474549
	φ	2.6740990	1.80481582	0.57409908
	λ	0.9791432	0.10594344	–0.02085683
210	δ	0.7251409	0.00430109	0.02514085
	φ	2.5078820	1.17924265	0.40788158
	λ	0.9724903	0.04517405	–0.02750967
280	δ	0.7202965	0.00278435	0.02029646
	φ	2.4308560	0.83369898	0.33085636
	λ	0.9650424	0.01788276	–0.03495761
350	δ	0.7146632	0.00199612	0.01466315
	φ	2.3374580	0.57413146	0.23745766
	λ	0.9735187	0.01219812	–0.02648126
420	δ	0.7086894	0.00118388	0.00868939
	φ	2.2400450	0.34417393	0.14004501
	λ	0.9847389	0.00667778	–0.01526112
490	δ	0.7054110	0.00058862	0.00541101
	φ	2.1926560	0.17625191	0.09265563
	λ	0.9879661	0.00384176	–0.01203392
560	δ	0.7033871	0.00036959	0.00338705
	φ	2.1610040	0.12874643	0.06100378
	λ	0.9923401	0.00315161	–0.00765986
630	δ	0.7041488	0.00044260	0.00414875
	φ	2.1339140	0.12976574	0.06391366
	λ	0.9916484	0.00228205	–0.00835155
700	δ	0.7025575	0.00023478	0.00255750
	φ	2.0862540	0.08124501	0.04625401
	λ	0.9933496	0.00151237	–0.00665041

* Set 1: $\delta = 0.7, \varphi = 2.1, \lambda = 1$.

Table 2. The simulation results of the GE-Weibull distribution.

n	Par.	MLE	MSEs	Biases
35	δ	0.9453885	0.01968309	0.04538846
	φ	2.8955960	3.79597445	0.69559603
	λ	1.7057310	2.06114888	0.50573079
70	δ	0.9369372	0.00990611	0.03693720
	φ	2.7763330	2.51574135	0.57633297
	λ	1.3626320	0.71742022	0.16263211
105	δ	0.9333706	0.00726861	0.03337062
	φ	2.8240060	2.18216357	0.62400620
	λ	1.2376500	0.31604070	0.03764968
140	δ	0.9292065	0.00515427	0.02920649
	φ	2.6870030	1.53044148	0.48700322
	λ	1.1826590	0.09967348	–0.01734086
210	δ	0.9222892	0.00318813	0.02228924
	φ	2.5900550	1.05587577	0.39005548
	λ	1.1605110	0.03559935	–0.03948925
280	δ	0.9142504	0.00196588	0.01425039
	φ	2.4536770	0.67126752	0.25367710
	λ	1.1768190	0.02793972	–0.02318052
350	δ	0.8913531	0.00134416	0.01135311
	φ	2.3993490	0.47376809	0.19934870
	λ	1.1747980	0.01387896	–0.02520224
420	δ	0.8879459	0.00084715	0.00794585
	φ	2.3344010	0.29290345	0.13440100
	λ	1.1809260	0.00766314	–0.01907393
490	δ	0.8646660	0.00051300	0.00466603
	φ	2.2741020	0.16139263	0.07410175
	λ	1.1902010	0.00492606	–0.00979894
560	δ	0.8546499	0.00050067	0.00464987
	φ	2.2490050	0.17555898	0.07900536
	λ	1.1889950	0.00521592	–0.01100532
630	δ	0.8313969	0.00014206	0.00139694
	φ	2.2334170	0.04508217	0.02341718
	λ	1.1967230	0.00153255	–0.00327667
700	δ	0.8115219	0.00014158	0.00152194
	φ	2.2162900	0.04783998	0.02629003
	λ	1.2157720	0.00116897	–0.00422816

* Set 2: $\delta = 0.8, \varphi = 2.2, \delta = 1, \lambda = 1.2$.

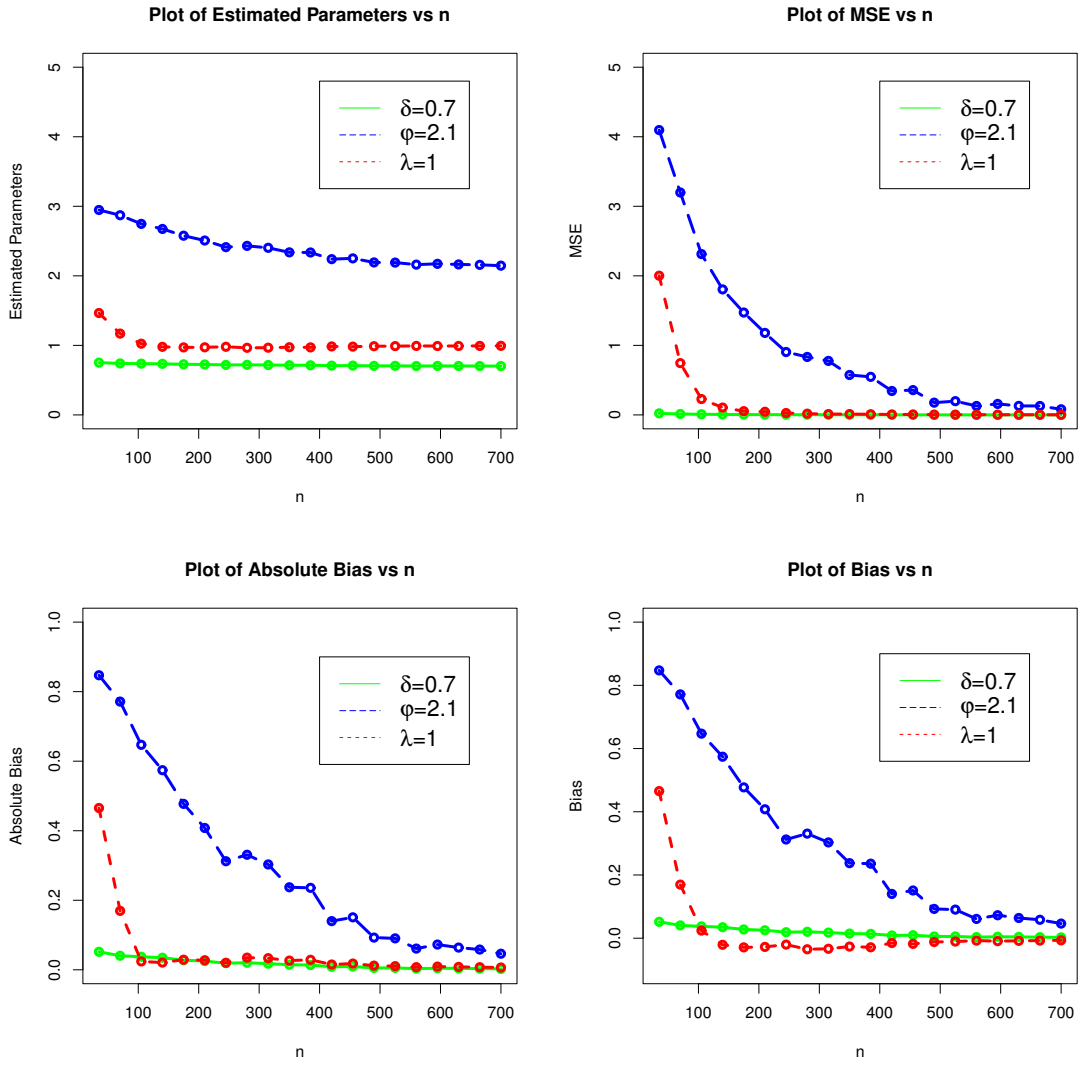

Figure 4. The simulation results for the GE-Weibull model for $\delta = 0.7, \varphi = 2.1, \lambda = 1$.

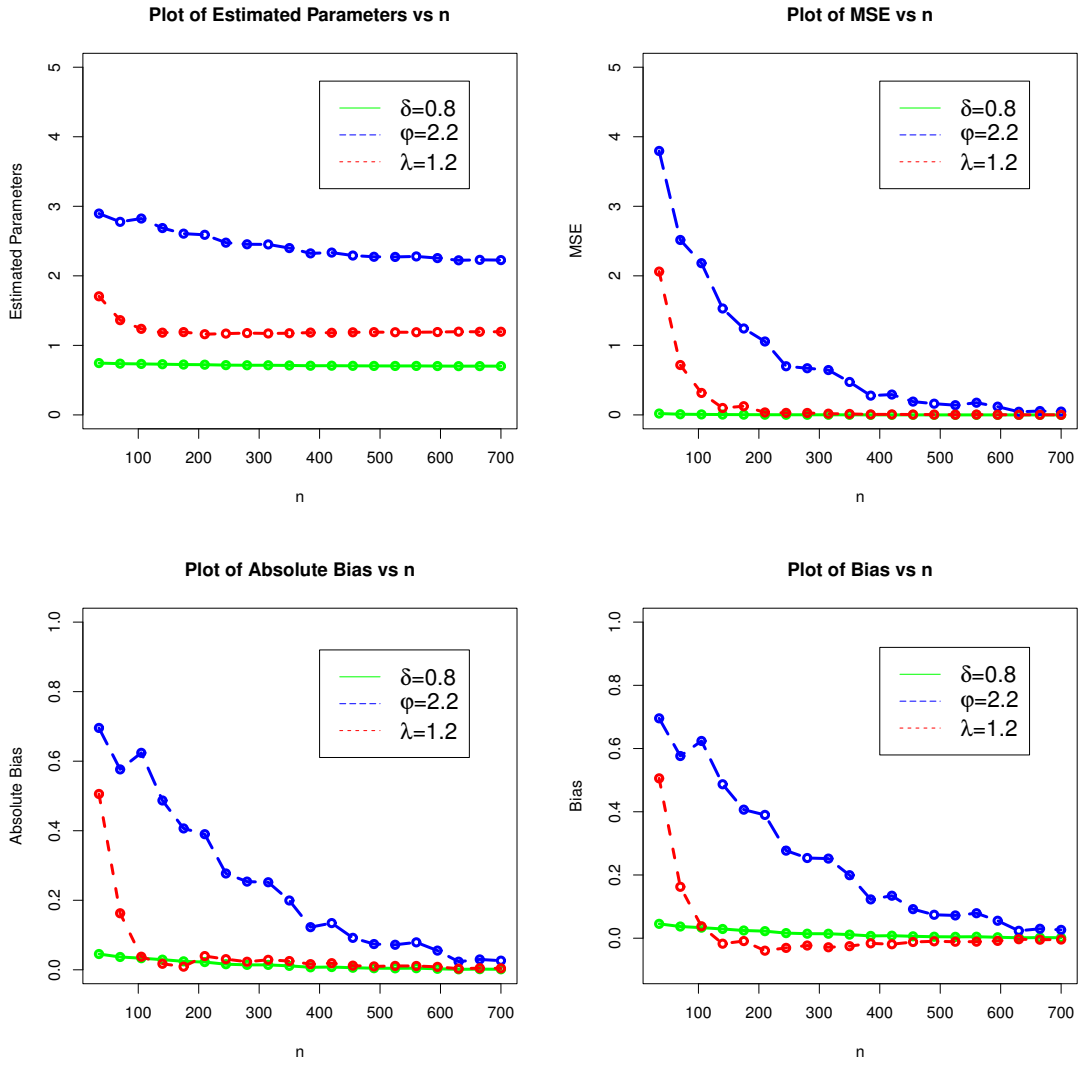

Figure 5. The simulation results for the GE-Weibull model for $\delta = 0.8, \varphi = 2.2, \delta = 1, \lambda = 1.2$.

6. Data analyses

As mentioned earlier, the modeling and prediction of the current pandemic are crucial and have attracted great interest from researchers. In this section, therefore, we describe the implementation of the GE-Weibull model to analyze three data sets.

- The initial data set consisted of the survival times (STs) observed in individuals diagnosed with COVID-19.
- The second and third data sets represent the mortality rates (MRs) of the patients (infected by COVID-19), and they were taken from Mexico and Holland, respectively.

All three data sets along with the respective references are provided in Table 3. The STs of the COVID-19 patients taken from China are expressed by x_1. Additionally, the MRs of the patients

selected from Mexico and Holland are expressed by x_2 and x_3, respectively. Some descriptive measures of the selected data sets are presented in Table 4. Furthermore, the plots corresponding to the selected data sets, namely the (*i*) box plots, (*ii*) histograms and (*iii*) total time on test (TTT) plots, are also shown in Figure 6. These plots reveal that the selected data sets are right-skewed and have some extreme observations. Alternatively, the TTT plots tell us about the behavior of the hazard rates. We refer interested readers to [32] for more information about the TTT plot.

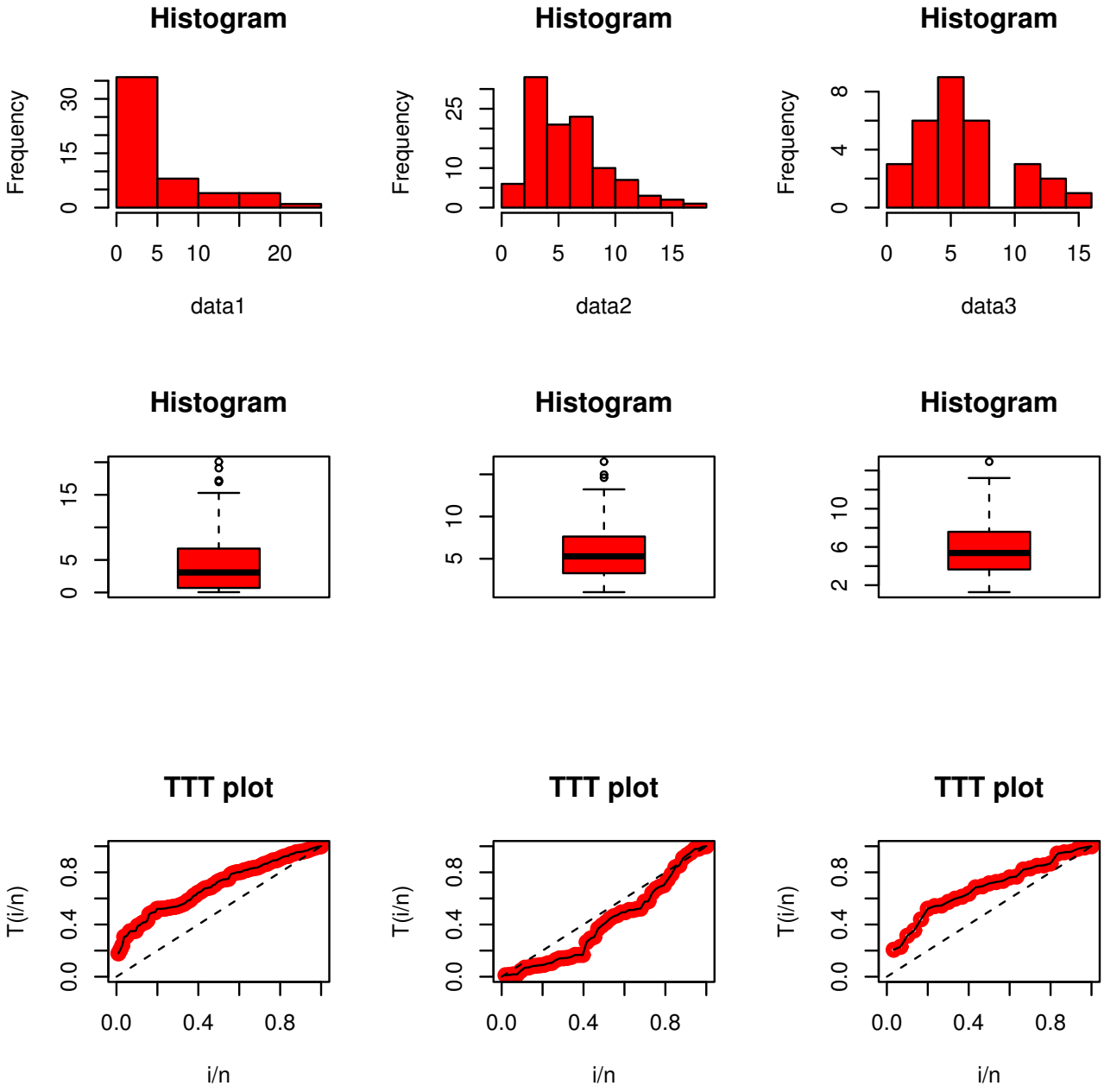

Figure 6. The histograms, box plots and TTT plots of the data sets.

Table 3. The COVID-19 data sets.

Notation	Observations	References
x_1	0.054, 0.064, 0.704, 0.816, 0.235, 0.976, 0.865, 0.364, 0.479, 0.568, 0.352, 0.978, 0.787, 0.976, 0.087, 0.548, 0.796, 0.458, 0.087, 0.437, 0.421, 1.978, 1.756, 2.089, 2.643, 2.869, 3.867, 3.890, 3.543, 3.079, 3.646, 3.348, 4.093, 4.092, 4.190, 4.237, 5.028, 5.083, 6.174, 6.743, 7.274, 7.058, 8.273, 9.324, 10.827, 11.282, 13.324, 14.278, 15.287, 16.978, 17.209, 19.092, 20.083	[33]
x_2	8.826, 6.105, 9.391, 14.962, 10.383, 7.267, 13.220, 16.498, 11.665, 6.015, 10.855, 6.122 , 6.656, 3.440, 5.854, 10.685, 10.035, 5.242, 4.344, 5.143, 7.630, 14.604, 7.903, 6.370, 3.537, 6.327, 4.730, 3.215, 9.284, 12.878, 8.813, 10.043, 7.260, 5.985 , 6.412, 3.395, 4.424, 9.935, 7.840, 9.550, 3.499, 3.751, 6.968, 3.286, 10.158, 8.108, 6.697, 7.151, 6.560, 2.077, 3.778, 2.988, 3.336, 6.814, 8.325, 7.854, 8.551, 3.228, 7.486, 6.625, 6.140, 4.909, 4.661, 5.392, 12.042, 8.696, 1.815, 3.327, 5.406, 6.182, 1.041, 1.800, 4.949, 4.089, 3.359, 2.070, 3.298, 5.317, 5.442, 4.557, 4.292, 2.500, 6.535, 4.648, 4.697, 5.459, 4.120, 3.922, 3.219, 1.402, 2.438, 3.257, 3.632, 3.233, 3.027, 2.352, 1.205, 3.218, 2.926, 2.601, 2.065, 3.029, 2.058, 2.326, 2.506, 1.923	[34]
x_3	14.918, 7.498, 6.940, 10.656, 2.857, 2.254, 12.274, 10.289, 10.832, 7.099, 3.461, 3.647, 5.928, 13.211, 7.968, 7.584, 5.307, 5.048, 5.431, 5.555, 6.027, 4.097, 3.611, 4.960, 4.462, 3.883, 1.974, 1.273, 1.416, 4.235	[34]

Table 4. Some descriptive measures of the data sets presented in Table 3.

Data	n	Mean	Median	Variance	Skewness	Kurtosis	Range
x_1	53	4.787	3.079	30.198	1.379	3.853	20.029
x_2	106	5.822	5.279	10.561	0.973	3.666	15.457
x_3	30	6.157	5.369	12.484	0.833	2.953	13.645

The fitting results for the GE-Weibull distribution have been compared with the Weibull distribution and its other prominent extensions. These distributions include the

- Weibull distribution,
- Kumaraswamy Weibull (K-Weibull) model of [35]
  and
- new alpha power cosine-Weibull (NAPC-Weibull) model of [36]. See for more references [37–39]

To obtain the analytical proof of the best fit of the competing models, four statistical tools were applied:

- Anderson-Darling (AD) test,
- Cramer-von Mises (CM) test,
- Kolmogorov-Smirnov (KS) test.

In addition to the aforesaid statistical tests, the p-values for all GE-Weibull and rival distributions were also calculated.

After analyzing the above data sets, the MLEs of the competing models were calculated as presented in Table 5. Furthermore, the values of the statistical tests for the fitted models are provided in Table 6. These results show that the GE-Weibull model is the most appropriate model to give the best fit to the COVID-19 data sets.

Using the COVID-19 data sets taken from China, Mexico and Holland, some empirical plots, namely, the estimated PDF, DF and Kaplan-Meier SF of the GE-Weibull model were derived as presented in Figures 7–9. The visual illustrations of the GE-Weibull model in Figures 7–9 also confirm its close-fitting capability as it pertains to the COVID-19 data sets.

Table 5. The values of $\hat{\delta}, \hat{\lambda}, \hat{\varphi}, \hat{a}, \hat{\tau}$ and $\hat{\alpha}$ of the fitted models.

Data	Models	$\hat{\delta}_{MLE}$	$\hat{\lambda}_{MLE}$	$\hat{\varphi}_{MLE}$	$\hat{a}_{MLE}$	$\hat{\tau}_{MLE}$	$\hat{\alpha}_{MLE}$
x_1	GE-Weibull	0.82272	0.27035	–7.78309	-	-	-
	Weibull	0.79022	0.32179	-	-	-	-
	K-Weibull	1.37571	0.01101	-	0.51340	3.07498	-
	NAPC-Weibull	0.79752	0.15065	-	-	-	0.52606
x_2	GE-Weibull	2.12658	0.01340	–3.00338	-	-	-
	Weibull	1.92306	0.02656	-	-	-	-
	K-Weibull	1.93559	0.15343	-	0.91662	0.16190	-
	NAPC-Weibull	1.47938	0.05112	-	-	-	4.11544
x_3	GE-Weibull	2.05602	0.01252	–2.35038	-	-	-
	Weibull	1.87110	0.02688	-	-	-	-
	K-Weibull	1.96043	0.17618	-	0.96010	0.12168	-
	NAPC-Weibull	1.47249	0.04644	-	-	-	3.79227

Table 6. The values of the analytical measures of the fitted models.

Data	Models	CM	AD	KS	p-value
x_1	GE-Weibull	0.074901	0.471266	0.119130	0.43940
	Weibull	0.07558	0.476885	0.125150	0.37760
	K-Weibull	0.075099	0.492309	0.126990	0.35980
	NAPC-Weibull	0.076949	0.481563	0.124750	0.38150
x_2	GE-Weibull	0.07921	0.50153	0.06185	0.81210
	Weibull	0.10241	0.65874	0.06986	0.67900
	K-Weibull	0.10990	0.71298	0.07773	0.53750
	NAPC-Weibull	0.13346	0.85822	0.06877	0.69220
x_3	GE-Weibull	0.03301	0.21613	0.08006	0.98230
	Weibull	0.04773	0.29327	0.09412	0.93050
	K-Weibull	0.05159	0.31394	0.11512	0.77960
	NAPC-Weibull	0.05670	0.34905	0.09940	0.89990

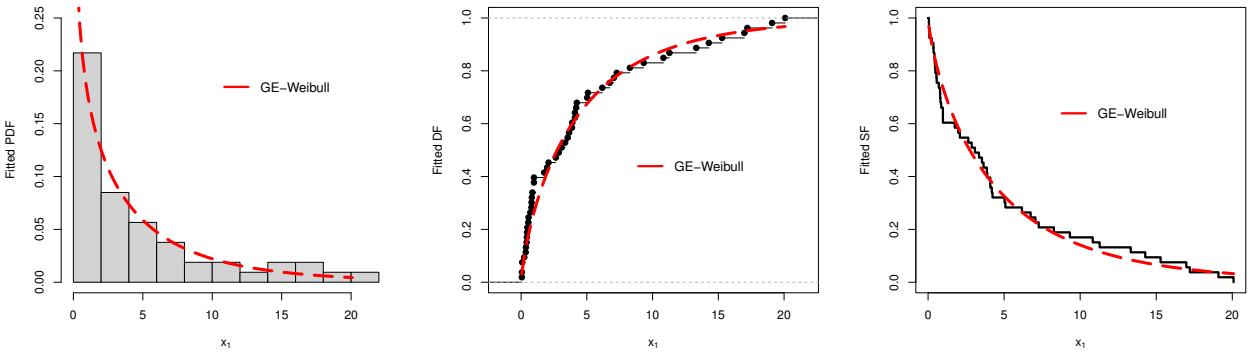

Figure 7. The plots of the fitted PDF, DF and SF of the GE-Weibull model for the STs of the COVID-19 patients taken from China.

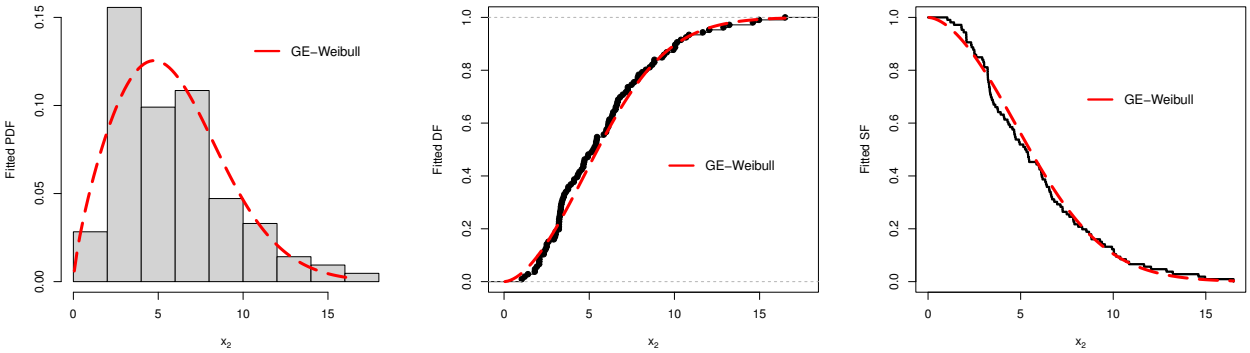

Figure 8. The plots of the fitted PDF, DF and SF of the GE-Weibull model for MRs of the COVID-19 patients taken from Mexico.

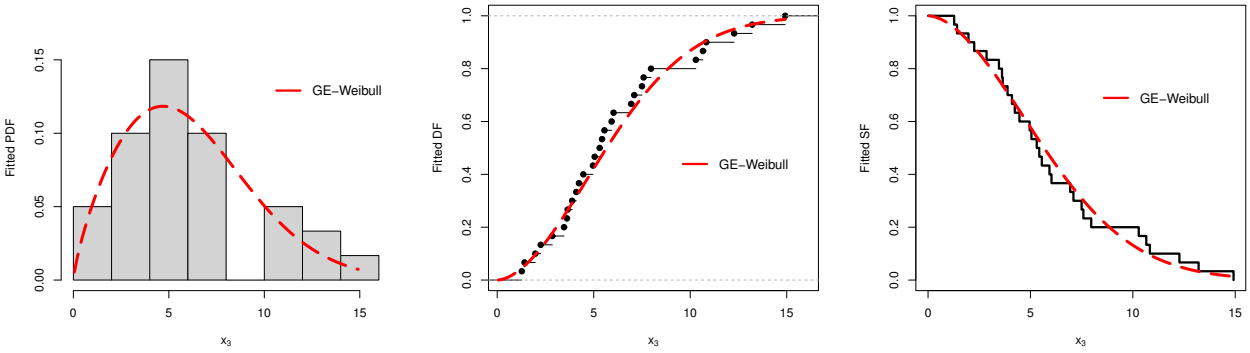

Figure 9. The plots of the fitted PDF, DF and SF of the GE-Weibull model for MRs of the COVID-19 patients taken from Holland.

7. Discussion

The HT distributions are significant to cater to the extreme observations. There are not many available probability distributions that possess the HT phenomena (i.e., characteristics and behaviors). Due to the crucial role of HT distributions in the medical sectors, we introduced a new method to obtain flexible extensions of the available probability distributions. The HT behavior of the suggested method is shown visually (see Figure 1) and mathematically (see Section 3). Based on the proposed GE-U family, a novel modification of the Weibull model has been considered and studied.

To demonstrate the practical use of the newly proposed GE-Weibull model, we examined its application on three medical data sets obtained from China, Holland and Mexico. The GE-Weibull distribution was applied to these data sets and its performance was compared against that of the traditional Weibull distribution and other notable extensions of the Weibull distribution, namely the K-Weibull and NAPC-Weibull distributions. We employed four widely recognized statistical evaluation criteria to assess the most appropriate model for the given medical data sets.

Upon thoroughly examining these datasets, we presented the numerical outcomes and fitted distributions of the GE-Weibull model in Table 6. Notably, for all three data sets, the information criterion values associated with the GE-Weibull distribution were consistently lower than for the other models. For x_1, the values of the statistical tests for the GE-Weibull model were given by CM = 0.074901, AD = 0.471266, KS = 0.119130 and p-value = 0.43940. For x_2, the values of the statistical tests for the GE-Weibull model were given by CM = 0.07921, AD = 0.50153, KS = 0.06185 and p-value = 0.81210. For x_3, the values of the statistical tests for the GE-Weibull model were given by CM = 0.03301, AD = 0.21613, KS = 0.08006 and p-value = 0.98230.

Since, for all three medical data sets, the GE-Weibull model performed better, we can conclude that the GE-Weibull distribution was the best and most-suited distribution to implement for these medical data sets.

8. Concluding remarks

This paper provides significant contributions to the advancement of distribution theory. A novel statistical method has been introduced and developed, enabling the generation of new probability distributions within the GE-U family. The MLEs for the GE-U distribution parameters has been derived. Building upon the GE-U family, a new model called the "GE-Weibull distribution" has been proposed. The HT characteristics of the GE-Weibull distribution were also investigated. To assess its performance, a comprehensive SiSt was conducted to evaluate the GE-Weibull distribution's parameter estimation. Additionally, the suitability of the GE-Weibull distribution was thoroughly examined by analyzing three distinct medical data sets from different countries: China, Holland and Canada. Based on specific information criteria, it was concluded that the GE-Weibull distribution was the most appropriate model for accurately representing and analyzing these medical data sets.

Use of AI tools declaration

The authors declare they have not used Artificial Intelligence (AI) tools in the creation of this article.

Acknowledgments

This research was supported by Princess Nourah bint Abdulrahman University Researchers Supporting Project number (PNURSP2023R368), Princess Nourah bint Abdulrahman University, Riyadh, Saudi Arabia.

Conflict of interest

The authors declare that there is no conflict of interest.

References

1. B. M. Batubara, The problems of the world of education in the middle of the Covid-19 pandemic, *BIRCI-J. Hum. Soc. Sci.*, 4 (2021), 450–457. https://doi.org/10.33258/birci.v4i1.1626
2. D. V. Parums, Long COVID, or post-COVID syndrome, and the global impact on health care. *Med. Sci. Monitor.*, 27 (2021), e933446-1–e933446-2. https://doi.org/10.12659/MSM.933446
3. M. K. Hassan, M. R. Rabbani, Y. Abdulla, Socioeconomic impact of COVID-19 in MENA region and the role of islamic finance, *Int. J. Islamic. Econ. Financ.*, 4 (2021), 51–78. https://doi.org/10.18196/ijief.v4i1.10466
4. A. K. Patel, S. Mukherjee, M. Leifels, R. Gautam, H. Kaushik, S. Sharma, O. Kumar, Mega festivals like MahaKumbh, a largest mass congregation, facilitated the transmission of SARS-CoV-2 to humans and endangered animals via contaminated water, *Int. J. Hyg. Envir. Heal.*, 237 (2021), 113836. https://doi.org/10.1016/j.ijheh.2021.113836
5. M. Škare, D. R. Soriano, M. Porada-Rochoń, Impact of COVID-19 on the travel and tourism industry, *Technol. Forecast. Soc.*, 163 (2021), 120469. https://doi.org/10.1016/j.techfore.2020.120469
6. S. Zondi, K. Ombongi, COVID-19, politics and international relations: hopes and impediments, *Politikon-UK.*, 48 (2021), 157–158. https://doi.org/10.1080/02589346.2021.1913800
7. S. M. Sayyd, Z. A. Zainuddin, P. M. Seraj, A scientific overview of the impact of COVID-19 pandemic on sports affairs: a systematic review, *Phys. Educ. stud.*, 25 (2021), 221–229. https://doi.org/10.15561/20755279.2021.0403
8. C. Strong, F. Cannizzo, Pre-existing conditions: Precarity, creative justice and the impact of the COVID-19 pandemic on the Victorian music industries, *Perfect. Beat.*, 21 (2021), 10–24. https://doi.org/10.1558/prbt.19379
9. S. Singh, R. Kumar, R. Panchal, M. K. Tiwari, Impact of COVID-19 on logistics systems and disruptions in food supply chain, *Int. J. Prod. Res.*, 59 (2021), 1993–2008. https://doi.org/10.1080/00207543.2020.1792000
10. C. Elleby, I. P. Domínguez, M. Adenauer, G. Genovese, Impacts of the COVID-19 pandemic on the global agricultural markets, *Environ. Resour. Econ.*, 76 (2020), 1067–1079. https://doi.org/10.1007/s10640-020-00473-6

11. M. Zuo, S. K. Khosa, Z. Ahmad, Z. Almaspoor, Comparison of COVID-19 pandemic dynamics in Asian countries with statistical modeling, *Comput. Math. Method. M.*, 2020 (2020), 4296806. https://doi.org/10.1155/2020/4296806
12. W. Bo, Z. Ahmad, A. R. A. Alanzi, A. I. Al-Omari, E. H. Hafez, S. F. Abdelwahab, The current COVID-19 pandemic in China: an overview and corona data analysis, *Alex. Eng. J.*, 61 (2022), 1369–1381. https://doi.org/10.1016/j.aej.2021.06.025
13. M. Campolieti, A. Ramos, The distribution of COVID-19 mortality, *Infect. Dis. Model.*, 7 (2022), 856–873. https://doi.org/10.1016/j.idm.2022.11.003
14. Á. Briz-Redón, Á. Serrano-Aroca, The effect of climate on the spread of the COVID-19 pandemic: a review of findings, and statistical and modelling techniques, *Prog. Phys. Geog.*, 44 (2020), 591–604. https://doi.org/10.1177/0309133320946302
15. I. Franch-Pardo, B. M. Napoletano, F. Rosete-Verges, L. Billa, Spatial analysis and GIS in the study of COVID-19. A review, *Sci. Total. Environ.*, 739 (2020), 140033. https://doi.org/10.1016/j.scitotenv.2020.140033
16. O. J. Peter, S. Qureshi, A. Yusuf, M. Al-Shomrani, A. A. Idowu, A new mathematical model of COVID-19 using real data from Pakistan, *Results. Phys.*, 24 (2021), 104098. https://doi.org/10.1016/j.rinp.2021.104098
17. A. I. Abioye, O. J. Peter, H. A. Ogunseye, F. A. Oguntolu, K. Oshinubi, A. A. Ibrahim, I. Khan, Mathematical model of COVID-19 in Nigeria with optimal control, *Results. Phys.*, 28 (2021), 104598. https://doi.org/10.1016/j.rinp.2021.104598
18. S. T. M. Thabet, M. S. Abdo, K. Shah, T. Abdeljawad, Study of transmission dynamics of COVID-19 mathematical model under ABC fractional order derivative, *Results. Phys.*, 19 (2020), 103507. https://doi.org/10.1016/j.rinp.2020.103507
19. U. I. Nwosu, C. P. Obite, Modeling Ivory Coast COVID-19 cases: identification of a high-performance model for utilization, *Results. Phys.*, 20 (2021), 103763. https://doi.org/10.1016/j.rinp.2020.103763
20. I. Rahimi, F. Chen, A. H. Gandomi, A review on COVID-19 forecasting models, *Neural. Comput. Appl.*, (2021). https://doi.org/10.1007/s00521-020-05626-8
21. M. Fatima, K. J. O'Keefe, W. Wei, S. Arshad, O. Gruebner, Geospatial analysis of COVID-19: a scoping review, *Int. J. Env. Res. Pub. He.*, 18 (2021), 2336. https://doi.org/10.3390/ijerph18052336
22. R. Kulik, P. Soulier, Heavy-tailed time series, *Springer Series in Operations Research and Financial Engineering*, New York: Springer-Verlag, 2020. https://doi.org/10.1007/978-1-0716-0737-4
23. M. A. Kouritzin, S. Paul, On almost sure limit theorems for heavy-tailed products of long-range dependent linear processes, *Stoch. Proc. Appl.*, 152 (2022), 208–232. https://doi.org/10.1016/j.spa.2022.06.021
24. W. Zhao, S. K. Khosa, Z. Ahmad, M. Aslam, A. Z. Afify, Type-I heavy tailed family with applications in medicine, engineering and insurance, *PLoS. One.*, 15 (2020), e0237462. https://doi.org/10.1371/journal.pone.0237462

25. D. Bhati, S. Ravi, On generalized log-Moyal distribution: a new heavy tailed size distribution, *Insur. Math. Econ.*, 79 (2018), 247–259. https://doi.org/10.1016/j.insmatheco.2018.02.002
26. Z. Li, J. Beirlant, S. Meng, Generalizing the log-Moyal distribution and regression models for heavy-tailed loss data, *ASTIN. Bull.*, 51 (2021), 57–99. https://doi.org/10.1017/asb.2020.35
27. A. Alzaatreh, C. Lee, F. Famoye, A new method for generating families of continuous distributions, *Metron.*, 71 (2013), 63–79. https://doi.org/10.1007/s40300-013-0007-y
28. Z. Ahmad, G. G. Hamedani, N. S. Butt, Recent developments in distribution theory: a brief survey and some new generalized classes of distributions, *Pak. J. Stat. Oper. Res.*, 15 (2019), 87–110. https://doi.org/10.18187/pjsor.v15i1.2803
29. H. A. Jessen, T. Mikosch, Regularly varying functions, *Publ. I. Math.*, 80 (2006), 171–192. https://doi.org/10.2298/PIM0694171H
30. E. Seneta, Karamata's characterization theorem, feller and regular variation in probability theory, *Publ, I. Math.*, 71 (2002), 79–89. https://doi.org/10.2298/PIM0271079S
31. S. I. Resnick, Heavy tail modeling and teletraffic data: special invited paper, *Ann. Stat.*, 25 (1997), 1805–1869. https://doi.org/10.1214/aos/1069362376
32. M. V. Aarset, How to identify a bathtub hazard rate, *IEEE. T. Reliab.*, 36 (1987), 106–108. https://doi.org/10.1109/TR.1987.5222310
33. X. Liu, Z. Ahmad, A. M. Gemeay, A. T. Abdulrahman, E. H. Hafez, N. Khalil, Modeling the survival times of the COVID-19 patients with a new statistical model: a case study from China. *PLoS. One.*, 16 (2021), e0254999. https://doi.org/10.1371/journal.pone.0254999
34. H. M. Almongy, E. M. Almetwally, H. M. Aljohani, A. S. Alghamdi, E. H. Hafez, A new extended rayleigh distribution with applications of COVID-19 data, *Results. Phys.*, 23 (2021), 104012. https://doi.org/10.1016/j.rinp.2021.104012
35. G. M. Cordeiro, E. M. Ortega, S. Nadarajah, The Kumaraswamy Weibull distribution with application to failure data, *J. Franklin. I.*, 347 (2010), 1399–1429. https://doi.org/10.1016/j.jfranklin.2010.06.010
36. A. S. Alghamdi, M. M. Abd El-Raouf, A new alpha power Cosine-Weibull model with applications to hydrological and engineering data, *Mathematics-Basel.*, 11 (2023), 673. https://doi.org/10.3390/math11030673
37. A. S. Hassan, S. G. Nassr, Power Lindly-G family of distribution, *Ann. Data. Sci.*, 6 (2019), 189–210. https://doi.org/10.1007/s40745-018-0159-y
38. A. S. Hassan, S. G. Nassr, The Inverse Weibull generator of distributions: properties and applications, *J. Data. Sci.*, 16 (2018), 723–742.
39. A. S. Hassan, S. G. Nassr, A new generalization of power function distribution: properties and estimation based on censored samples, *Thail. Statiet.*, 18 (2020), 215–234.

Appendix A

Here, we provide the step-by-step derivation of the expression provided in Eq (2.2). Using $M\left[U\left(x;\boldsymbol{\psi}\right)\right] = -\log\left(\frac{\varphi^2\left[1-U(x;\boldsymbol{\psi})\right]}{\left[\varphi-U(x;\boldsymbol{\psi})\right]^2}\right)$, by taking ϕ_1 as the lower limit of the exponential distribution with

the PDF $w(t) = e^{-t}$ in Eq (2.1), we get

$$K(x;\varphi,\boldsymbol{\psi}) = \int_0^{-\log\left(\frac{\varphi^2[1-U(x;\boldsymbol{\psi})]}{[\varphi-U(x;\boldsymbol{\psi})]^2}\right)} e^{-t}\, dt,$$

$$K(x;\varphi,\boldsymbol{\psi}) = -e^{-t}\Big|_0^{-\log\left(\frac{\varphi^2[1-U(x;\boldsymbol{\psi})]}{[\varphi-U(x;\boldsymbol{\psi})]^2}\right)},$$

$$K(x;\varphi,\boldsymbol{\psi}) = -\left(e^{\log\left(\frac{\varphi^2[1-U(x;\boldsymbol{\psi})]}{[\varphi-U(x;\boldsymbol{\psi})]^2}\right)} - e^{-0}\right),$$

$$K(x;\varphi,\boldsymbol{\psi}) = -\left(\frac{\varphi^2\left[1-U(x;\boldsymbol{\psi})\right]}{\left[\varphi-U(x;\boldsymbol{\psi})\right]^2} - 1\right),$$

$$K(x;\varphi,\boldsymbol{\psi}) = 1 - \frac{\varphi^2\left[1-U(x;\boldsymbol{\psi})\right]}{\left[\varphi-U(x;\boldsymbol{\psi})\right]^2},$$

$$K(x;\varphi,\boldsymbol{\psi}) = 1 - \frac{\varphi^2\bar{U}(x;\boldsymbol{\psi})}{\left[\varphi-U(x;\boldsymbol{\psi})\right]^2}$$

Appendix B

Here, we provide the R code that we used to obtain the plots for the DF and SF of the proposed model. In the given R code, we have used v for φ, lam for λ and del for δ.

```
#########################################################################
R code for obtaining the plot of the DF of the GE-Weibull distribution
#########################################################################
x=seq(0, 5, 0.01);
dis=function(x, v, lam, del)
1-((v^2)*exp(-lam*x^del)/((v-1+exp(-lam*x^del))^2))
a=dis(x,2.5, 1.6, 1.8)
a
plot(x,a,type="l",col="red",lwd=4, lty=8, xlab="x", ylab="K(x)")
legend(1.5,0.5, legend = c(expression(paste(delta," = ","1.8, ",lambda,
" = ","1.6, ",varphi," = ",2.5))), lty =c(1,5,8),cex=1.1,
col=c('red'),box.lty=0)
#########################################################################
R code for obtaining the plot of the SF of the GE-Weibull distribution
#########################################################################

x=seq(0, 5, 0.01);
dis=function(x, v, lam, del)
((v^2)*exp(-lam*x^del)/((v-1+exp(-lam*x^del))^2))
```

```
a=dis(x,2.5, 1.6, 1.8)
a
plot(x,a,type="l",col="red",lwd=4, lty=8, xlab="x", ylab="S(x)")
legend(1.5,0.5, legend = c(expression(paste(delta," = ","1.8, ",lambda,
" = ","1.6, ",varphi," = ",2.5))), lty =c(1,5,8),cex=1.1,
col=c('red'),box.lty=0)
```

AIMS Press